Transient Spectral Features of a cis−trans Photoreaction in the Condensed Phase: A Model Study

Birgit Balzer and Gerhard Stock*

Institute of Physical and Theoretical Chemistry, J. W. Goethe University, Marie-Curie-Strasse 11, D-60439 Frankfurt, Germany

Received: March 8, 2004; In Final Form: May 4, 2004

A theoretical description to calculate transient absorption spectra of photoreactive systems in the condensed phase is developed. The formulation comprises a multidimensional model of nonadiabatic photoisomerization, a Redfield treatment of the environment within the secular approximation, and a doorway−window formulation to calculate transient pump−probe spectra. Employing the eigenstate representation and assuming Gaussian laser pulses, we derive explicit expressions for the doorway and window operators. The formalism scales with N^2 (N being the dimension of the system Hamiltonian matrix) and therefore allows us to handle multidimensional molecular models. Detailed computational studies of the dynamics and transient absorption are presented for various cis−trans photoisomerization models. It is shown that only the two-mode model involving a conical intersection yields short-time transients, as expected for a condensed-phase system. Problems in the interpretation of transient spectra associated with the competition (and cancellation) of the various spectroscopic contributions in a photoreaction are discussed in some detail. The computational studies demonstrate the need for theoretical modeling in order to achieve a microscopic interpretation of femtosecond experiments.

1. Introduction

Ever since femtosecond lasers became available to researchers in chemical physics, ultrafast laser pulses have been employed as a "real-time camera" to observe elementary photochemical processes.[1] Most of these experiments are of the pump−probe type; that is, at time $t = 0$ the molecular system is prepared by the first pulse (the pump) into a nonstationary state, the time evolution of which is interrogated by a second pulse (the probe) at time $t = \Delta t$. An important class of photoreactions, which has successfully been investigated by femtosecond spectroscopy, is cis−trans photoisomerization.[2,3] Examples include small molecules in the gas phase such as ethene[4] and organic photoswitches such as azobenzene[5] up to photoactive proteins such as rhodopsin.[6] To illustrate the spectroscopic response of a cis−trans photoisomerization reaction, Figure 1 schematically shows the potential-energy curves of such a system, plotted as a function of the torsional reaction coordinate φ. Following the photoexcitation of the molecule at time $t = 0$, the system may undergo cis → trans isomerization (solid arrows) as well as back-reaction to the cis configuration (dotted arrow). Employing a time-delayed laser pulse to probe the dynamics, we find that at early times the photoinduced excited-state population gives rise to stimulated emission and excited-state absorption. However, the reduced population in the electronic ground state causes a bleach of the cis absorption band as well as stimulated impulsive Raman scattering. At later times, the transient spectrum is dominated by the absorption of the photoproduct in the trans configuration and by the absorption of the recovered reactant in the cis configuration. Because the spectral bands associated with the various processes typically overlap (at least partly) and because the positive (by convention) absorption signal and the negative emission signal cancel each other, the interpretation of transient transmission experiments is a nontrivial problem that strongly depends on theoretical support. Moreover, the interpretation may be supported by complementary experimental techniques including (for the example of bacteriorhodopsin) time-resolved fluorescence[7] and Raman[8] spectroscopy, infrared probing,[9] multipulse techniques,[10] and photon echo experiments[11] as well as ultrafast spectroscopy on modified chromophores.[12] In particular, the detection of the fluorescence allows to study the emission from the excited electronic state exclusively and therefore monitors directly the decay of the excited-state population.

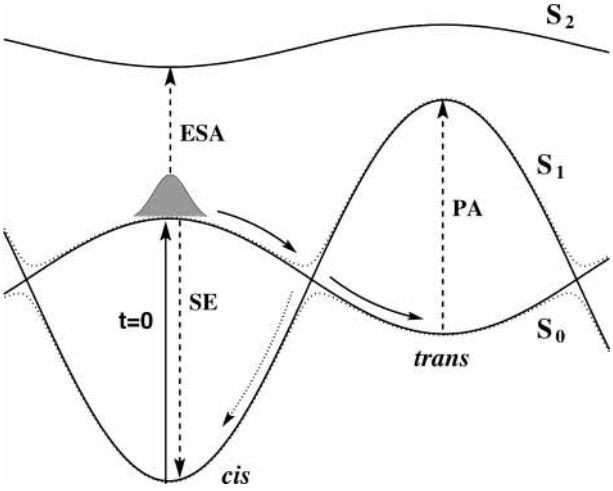

Figure 1. Scheme of the diabatic (solid line) and adiabatic (dotted line) potential-energy curves of the cis−trans photoisomerization model under consideration. Following photoexcitation of the system at a wavelength of 500 nm, the system may undergo cis → trans isomerization (solid arrows) as well as a back reaction to the cis configuration (dotted arrow). Probing the system by a second time-delayed laser pulse initially gives rise to stimulated emission (SE), excited-state absorption (ESA), and a bleach of the ground state. At later times, the transient spectrum exhibits photoproduct absorption (PA) at a wavelength of ∼570 nm as well as the absorption of the recovered reactant at 500 nm.

A suitable theoretical description of the time-resolved spectroscopy of cis−trans photoreactions has to take into account

* Corresponding author. E-mail: stock@theochem.uni-frankfurt.de.

10.1021/jp048965i CCC: $27.50
Published on Web 07/14/2004

several issues. First, it is well established that the twisting of a double bond typically leads to an electronic curve crossing, which causes nonadiabatic relaxation of the system from the electronic excited-state back to the ground state.[2,3] Extensive ab initio studies have shown that this ultrafast internal conversion process typically involves several accepting modes (say, one to three apart from the reaction coordinate), which need to be considered in the calculation.[13,14] Second, an appropriate description needs to account for the subsequent vibrational cooling of the photoproducts (i.e., the vibrational energy redistribution between the initially excited modes and the remaining degrees of freedom). This is because vibrational cooling stops the system from oscillating between the coupled states and is responsible for the localization of the molecule in a specific configuration. Finally, the interaction of the system with the laser pulses should be described explicitely (i.e., either by perturbative calculations,[15] with respect to matter−field coupling, or by a nonperturbative simulation of the experiment[16]).

Although there have been numerous works in each of the topics listed above, it is difficult to account for all three issues in the same formulation (i.e., to combine a multidimensional nonadiabatic molecular system with dissipative coupling to the environment and an explicit treatment of the laser−molecule interaction). On one hand, a multidimensional model system results in a large dimension N of the Hamiltonian matrix. On the other hand, the numerical effort of a Redfield treatment of dissipation (i.e., a reduced density-matrix description that assumes weak system−bath coupling and the Markov approximation for the bath response[17,18]) scales with N^3, which in practice means that $N \lesssim 10^3$. Similarly, a standard nonperturbative treatment of the matter−field interaction scales with N^3, and eigenstate-free perturbative expressions that contain multiple-time response functions are usually even more cumbersome to evaluate.[14] For this reason, explicit calculations of pump−probe spectra for dissipative systems have so far been performed only for a few systems, including the damped harmonic oscillator (which gives analytic response functions)[19] and various exciton and electron-transfer systems.[20−24]

To facilitate a generally applicable description of nonlinear spectroscopy for a system requiring a large dimension N of the system Hamiltonian, it would be clearly advantageous to invoke suitable approximations such that the resulting method merely scales with N^2. In the Redfield formulation, for example, one may adopt the secular approximation,[17,18] which retains only the secular (i.e., resonant) terms of the Redfield tensor. As a consequence of this assumption, only the diagonal elements of the reduced density matrix need to be evaluated numerically (i.e., the propagation of the Redfield equation scales with N^2 [25]). To reduce the numerical effort of the spectroscopic calculations, it is often assumed that the pump and probe laser pulses do not overlap in time. On the basis of this assumption, several formulations to calculate nonlinear spectra have been proposed, including the semiclassical Franck−Condon principle,[26] a convolution scheme,[14] and the so-called doorway−window representation.[27] Whereas the first two methods are wave function formulations that allow for an eigenstate-free evaluation, the latter represents a density-operator formulation that facilitates the inclusion of dissipation. Moreover, assuming exponential pulse shapes and introducing the eigenstates of the system Hamiltonian, it has recently been shown that the evaluation of the doorway and window operators also scales with N^2.[24] Because the numerical propagation of the Redfield equation is usually performed in the eigenstate representation anyway, there is no major additional effort when combining the doorway−window and secular Redfield formulations.

In this work, a theoretical study of the femtosecond transient absorption of a cis−trans photoreaction is presented. The formulation consists of the following parts: (i) A recently proposed model of nonadiabatic isomerization that takes into account two coupled electronic states, one reaction coordinate, and one vibronically active mode;[28,29] (ii) a Redfield treatment of dissipation within the secular approximation; and (iii) a doorway−window formulation to calculate transient pump−probe spectra. Employing the eigenstate representation and assuming Gaussian laser pulses, we derived explicit expressions for the doorway and window operators. The validity and accuracy of the formulation are checked by a comparison to (numerically) exact nonperturbative reference calculations. The remainder of the paper is concerned with a detailed numerical study of the transient spectral features of cis−trans photoisomerization as monitored in a femtosecond pump−probe experiment. The analysis considers both the short- and the long-time evolution of the spectra. Problems with the interpretation of transient spectra due to the competition (and cancellation) of the various spectroscopic contributions in a photoreaction are discussed in some detail.

2. Theoretical Formulation

2.1. Model System. To describe the dissipative dynamics of a photoisomerization reaction, the usual system−bath approach is employed in which the molecular Hamiltonian

$$H_{\mathrm{M}} = H_{\mathrm{S}} + H_{\mathrm{B}} + H_{\mathrm{SB}} \tag{2.1}$$

is partitioned into the system Hamiltonian H_S representing the isomerizing chromophore including the vibrational modes directly involved in the reaction, the bath Hamiltonian H_{B} comprising the remaining modes of the chromophore and the environment, and the coupling H_{SB} between the system and the environment.

Following earlier work,[28,29] we assume that the main aspects of the cis−trans photoisomerization can be modeled by an electronic two-state system. Adopting a diabatic electronic representation with the diabatic electronic ground state $|\psi_0\rangle$ and the first excited state $|\psi_1\rangle$, the system Hamiltonian is given as the sum of the kinetic energy T and the diabatic potential matrix $\{V_{nm}\}$

$$H_{\mathrm{S}} = \sum_{n=0,1,2} |\psi_n\rangle(T + V_{nn})\langle\psi_n| + \{|\psi_0\rangle V_{01}\langle\psi_1| + \text{h.c.}\} \tag{2.2}$$

where the second excited electronic state $|\psi_2\rangle$ is included to account for the $|\psi_1\rangle \rightarrow |\psi_2\rangle$ excited-state absorption. In this paper, results will be given for two models of nonadiabatic photoisomerization: the simplest case including a single reaction coordinate φ as well as a more realistic two-mode model that additionally contains a vibrational coordinate q that collectively accounts for all vibronically active modes. The models differ also in the diabatic coupling $V_{01} = V_{10}$. For the single-mode model, the diabatic coupling is constant, $V_{01} = \lambda_0$, but the coupling of the two-mode model is coordinate-dependent, $V_{01} = \lambda q$. As a consequence, the adiabatic potential-energy curves of the single-mode model exhibit an avoided crossing at $\varphi = {}^{\pi}/_{2}$, whereas the potential-energy surfaces of the two-mode model exhibit a conical intersection, also called a "photochemical funnel", which causes a fast and efficient isomerization process.[3] It is noted that the latter model was originally designed to reproduce the transient absorption of retinal in rhodopsin.[28]

Representing the torsional motion along the reaction coordinate in terms of cosine functions and employing the harmonic approximation for the vibrational mode q, the matrix elements of the Hamiltonian are given as[29]

$$T = -\frac{1}{2I}\frac{\partial^2}{\partial\varphi^2} - \frac{\omega}{2}\frac{\partial^2}{\partial q^2} \tag{2.3a}$$

$$V_{nn} = E_n + \frac{1}{2}\tilde{V}_n(1 - \cos\varphi) + \frac{\omega}{2}q^2 + \delta_{1n}\kappa q \tag{2.3b}$$

where dimensionless coordinates and $\hbar \equiv 1$ are employed. In the case of the single-mode model, all terms containing q in eq 2.1 are neglected. Following refs 28 and 30, the parameters of the models are (in eV) $I^{-1} = 4.84 \times 10^{-4}$, $E_0 = 0.0$, $E_1 = 2.48$, $E_2 = 4.91$, $\tilde{V}_0 = 3.6$, $\tilde{V}_1 = -1.09$, $\tilde{V}_2 = 2.0$, $\omega = 0.19$, $\kappa = 0.095$, $\lambda = 0.19$, and $\lambda_0 = 0.065$.

2.2. Dissipative Dynamics. As is common practice, the bath is described within the harmonic approximation

$$H_B = \sum_\alpha \frac{\omega_\alpha}{2}(x_\alpha^2 + p_\alpha^2) \tag{2.4}$$

where x_α and p_α represent the position and momentum operators pertaining to the αth vibrational mode, respectively. For the system−bath coupling, we choose[30]

$$H_{SB}^T = |\psi_1\rangle\langle\psi_1|\sum_\alpha g_{\varphi,\alpha}(1 - \cos\varphi)x_\alpha + g_{q,\alpha}qx_\alpha \tag{2.5a}$$

$$H_{SB}^C = |\psi_0\rangle\langle\psi_0|\sum_\alpha g_{\varphi,\alpha}(1 + \cos\varphi)x_\alpha + g_{q,\alpha}qx_\alpha \tag{2.5b}$$

$$H_{SB}^S = \frac{1}{2}(H_{SB}^T + H_{SB}^C) \tag{2.5c}$$

Because $(1 - \cos\varphi)$ is maximal for $\varphi = \pm\pi$, for H_{SB}^T the bath couples predominantly to the trans configuration. Furthermore, the projection onto the diabatic state $|\psi_1\rangle$ affects the coupling to the adiabatic ground state in the trans configuration. (Remember that the diabatic potential-energy surfaces are inverted in eq 2.3b.) Hence, H_{SB}^T predominantly affects the localization of the system in its ground-state trans configuration. Similarly, H_{SB}^C leads to a preferred localization of the system in its ground-state cis configuration. As a third case, a symmetric coupling H_{SB}^S is considered, in which the bath couples to both the cis and the trans configurations, respectively. The coupling constants $g_{\varphi,\alpha}$ and $g_{q,\alpha}$ are chosen according to an Ohmic spectral density

$$J_i(\omega) = \frac{\pi}{2}\sum_\alpha g_{i,a}^2\delta(\omega - \omega_\alpha) = \eta_i\omega e^{-\omega/\omega_{c,i}} \qquad (i = \varphi, q) \tag{2.6}$$

Here the overall strength of the system−bath coupling is given by the dimensionless parameter η_i, and the cutoff frequency $\omega_{c,i}$ describes the time-scale distribution of the bath. The parameters for the single-mode model are chosen as $\eta_\varphi = 0.45$ and $\omega_{c,\varphi} = 0.035$ eV, and for the two-mode model, we assume that $\eta_\varphi = 0.025$, $\omega_{c,\varphi} = 0.035$ eV, $\eta_q = 0.025$, and $\omega_{c,q} = 0.19$ eV.[31]

To describe the dissipative dynamics of the system, we employ the Redfield approach, that is, a second-order perturbation theory with respect to the system−bath interaction combined with a Markov approximation for the relaxation operators.[17,18] Adopting the system eigenstate representation, $H_S|l\rangle = E_l|l\rangle$, the Redfield equation is given as

$$\frac{\partial}{\partial t}\sigma_{ij} = -i\omega_{ij}\sigma_{ij} + \sum_{k,l} R_{ijkl}\sigma_{kl} \tag{2.7}$$

where σ denotes the reduced density matrix, $\omega_{ij} = E_i - E_j$, and R_{ijkl} represents the Redfield relaxation tensor, which describes the interaction of the molecular system with the bath. As a further simplification, we employ the secular approximation, which considers only the resonant terms of the Redfield tensor R_{ijkl}, that is, terms satisfying $\omega_{ij} - \omega_{kl} = 0$.[17,18] The secular approximation affects a decoupling of the diagonal and off-diagonal elements of σ and therefore leads to an N^2 scaling of the reduced density-matrix propagation. Various studies have shown that this approximation tends to suppress vibrational coherences at early propagation times.[30,32,33] As shown in ref 30, however, the secular approximation is well justified for the present single-mode model. In the case of the two-mode model, the secular approximation underestimates the oscillations at early times, yet the long-time dynamics is still described correctly. Because we are especially interested in monitoring the cooling process to a preferred molecular configuration after photoexciting the molecule, it is therefore justifiable to employ the secular approximation. A more detailed discussion of the validity of the secular approximation for various multidimensional isomerization models is given in ref 25.

2.3. Definition of Spectroscopic Signals. To describe a spectroscopic experiment, the total Hamiltonian is written as

$$H(t) = H_M + H_{int}(t) \tag{2.8}$$

where

$$H_{int}(t) = -\mu E(t) \tag{2.9}$$

accounts for the interaction of the molecular system with the radiation field within the dipole approximation. The electronic transition dipole moment operator can be written as

$$\mu = \sum_{i\neq j}|i\rangle\mu_{ij}\langle j| \tag{2.10}$$

where μ_{ij} is the Franck−Condon factor for the electronic transition between eigenstates $|i\rangle$ and $|j\rangle$ associated with different electronic states. The external electric field $E(t)$ is defined by

$$E(t) = E_1(t) + E_2(t) + \text{c.c.} \tag{2.11a}$$

$$E_i(t) = \frac{\epsilon_i}{\sqrt{4\pi\alpha\tau_i}}e^{-(t - t_i)^2/(4\alpha\tau_i^2)}e^{-i\omega_i(t - t_i)} \tag{2.11b}$$

with $\alpha = 1/(16\ln 2)$. Gaussian-shaped pump and probe pulses $E_1(t)$ and $E_2(t)$ are characterized by their carrier frequencies ω_1 and ω_2 and their durations τ_1 and τ_2, respectively. They are centered at times $t = t_i$, where $t_1 = 0$ and $t_2 = \Delta t$, representing the delay time of the probe pulse.

The key quantity in the calculation of spectroscopic signals is the electric polarization of the system, which is given as the expectation value of the electronic transition dipole operator

$$P(t) = \text{Tr}\{\sigma(t)\mu\} \tag{2.12}$$

In this work we are concerned with the differential absorption spectrum that is calculated from the polarization induced by both the pump and probe pulses minus the polarization induced by the probe pulse. Usually, two different detection schemes are employed to measure the probe absorption. In the first scheme, the total (i.e., frequency-integrated) intensity of the

probe field is measured as a function of the probe center frequency ω_2 and the delay time Δt. Employing the rotating-wave approximation and the slowly varying amplitude approximation,[15] we thus obtain

$$I(\omega_2, \Delta t) = 2\omega_2 \mathrm{Im} \int_{-\infty}^{\infty} \mathrm{d}t\, E_2(t)\, P^*(t) \qquad (2.13)$$

which will be referred to as integral pump−probe signal. The sign convention is such that the signal is positive for absorption (gain of energy by the system) and negative for emission and bleach (loss of energy by the system). Alternatively, the probe center frequency ω_2 is fixed, and the probe field is dispersed after the sample by a monochromator. Considered to be a function of the dispersed frequency ω and the delay time Δt, the corresponding dispersed pump−probe signal (or transient absorption spectrum) is given by[14]

$$S(\omega, \Delta t) = 2\omega \mathrm{Im}\, E_2(\omega)\, P^*(\omega) \qquad (2.14)$$

where $E_2(\omega)$ and $P(\omega)$ denote the Fourier transforms of the probe pulse and the polarization, respectively. We note that the experimental absorption spectrum is often normalized with respect to the incident probe intensity $|E_2(\omega)|^2$.

2.4. Nonperturbative Calculation of the Polarization. A straightforward approach to simulate femtosecond pump−probe experiments is the direct propagation of the Liouville equation including the total Hamiltonian (eq 2.8):

$$\frac{\partial}{\partial t}\sigma(t) = -\mathrm{i}[H(t), \sigma(t)] \qquad (2.15)$$

This method is well established for the wave function formalism[29,16] and was also extended to a density-matrix description.[20] In contrast to the commonly applied perturbation theory, this approach is obviously applicable for any strength of the laser fields. Within the Redfield formulation, eq 2.15 becomes

$$\frac{\partial}{\partial t}\sigma_{ij} = -\mathrm{i}\omega_{ij}\sigma_{ij} + \sum_{k,l} R_{ijkl}\sigma_{kl} + \mathrm{i}E(t)\sum_k (\mu_{ik}\sigma_{kj} - \mu_{kj}\sigma_{ik}) \qquad (2.16)$$

The last term in eq 2.16 implies an N^3 scaling, which makes the nonperturbative approach to pump−probe spectra within Redfield theory computationally expensive for large N. Furthermore, a nonperturbative calculation yields the total polarization (eq 2.12), whereas for interpretative purposes one is interested in discriminating the various spectral contributions of the polarization. In the present work, for example, we focus on emission in the direction of the probe pulse and wish to discriminate contributions originating from the ground state (i.e., bleach and stimulated Raman) and from the excited state (i.e., stimulated emission and excited-state absorption). For nonadiabatically coupled systems, an additional complication arises: one needs to distinguish whether an electronic transition is caused by vibronic interactions or via the coupling to the radiation field. In the case of the vibronic-coupling model system (eq 2.2), it is necessary to extend the decomposition scheme developed in ref 16; see Appendix A.

2.5. Doorway−Window Representation. Using time-dependent perturbation theory and assuming nonoverlapping pump and probe pulses, Yan and Mukamel[27] showed that the pump−probe signal (eq 2.13) can be written in the form

$$I(\omega_2, \Delta t) = 2\omega_2 \mathrm{Tr}\{W(\omega_2) \mathrm{e}^{-\mathrm{i}\mathcal{L}_\mathrm{M}\Delta t} D(\omega_1)\} \qquad (2.17)$$

Here, $D(\omega_1)$ denotes the doorway operator describing the preparation of the system at time $t = 0$ by the pump pulse, $\mathcal{L}_\mathrm{M}\cdots = [H_\mathrm{M}, \cdots]$ is the molecular Liouvillian accounting for the dissipative time evolution of the molecular system during $0 \le t \le \Delta t$, and $W(\omega_2)$ represents the window operator describing the interaction of the system with the probe laser at $t = \Delta t$.

To obtain expressions for the doorway and window operators that are useful in practice, it is convenient to neglect the system−bath coupling during the interaction of the system with the laser fields. This approximation is justified for pulses that are short compared to the time scale of the bath-induced relaxation. It is noted, however, that between the interaction with the pump pulse and the interaction with the probe pulse (i.e., during the delay time Δt) system−bath coupling is taken into account by solving the Redfield equation (eq 2.7).

Within these assumptions, the doorway operator can be written as $D(\omega_1) = D_e(\omega_1) + D_g(\omega_1)$, with[15,27]

$$D_e(\omega_1) = \int_{-\infty}^{\infty} \mathrm{d}t' \int_0^{\infty} \mathrm{d}t_1\, E^*{}_1(t')\, E_1(t' - t_1) \times [\mathrm{e}^{\mathrm{i}H_S t'} \mathrm{e}^{-\mathrm{i}H_S t_1} \mu \sigma^{\mathrm{eq}} \mathrm{e}^{\mathrm{i}H_S t_1} \mu \mathrm{e}^{-\mathrm{i}H_S t'}] + \mathrm{h.c.} \qquad (2.18)$$

$$D_g(\omega_1) = \int_{-\infty}^{\infty} \mathrm{d}t' \int_0^{\infty} \mathrm{d}t_1\, E^*{}_1(t')\, E_1(t' - t_1) \times [\mathrm{e}^{\mathrm{i}H_S t'} \mu \mathrm{e}^{-\mathrm{i}H_S t_1} \mu \sigma^{\mathrm{eq}} \mathrm{e}^{\mathrm{i}H_S t_1} \mathrm{e}^{-\mathrm{i}H_S t'}] + \mathrm{h.c.} \qquad (2.19)$$

where $\sigma^{\mathrm{eq}} = \sigma(-\infty)$ describes the initial system in thermal equilibrium. As is well known, the interaction with the pump pulse creates a "particle" in the excited electronic state described by $D_e(\omega_1)$ and a "hole" in the ground electronic state represented by $D_g(\omega_1)$. In the measured spectroscopic signal (eq 2.13), $D_e(\omega_1)$ leads to stimulated emission, excited-state absorption, and photoproduct absorption, and $D_g(\omega_1)$ gives rise to the ground-state bleach and the stimulated Raman contribution.

The window operator can be written as

$$W(\omega_2) = \int_{-\infty}^{\infty} \mathrm{d}t \int_0^{\infty} \mathrm{d}t_3\, E^*{}_2(t + t_3)\, E_2(t) \times [\mathrm{e}^{\mathrm{i}H_S t} \mathrm{e}^{\mathrm{i}H_S t_3} \mu \mathrm{e}^{-\mathrm{i}H_S t_3} \mu \mathrm{e}^{-\mathrm{i}H_S t} - \mathrm{e}^{\mathrm{i}H_S t} \mu \mathrm{e}^{\mathrm{i}H_S t_3} \mu \mathrm{e}^{-\mathrm{i}H_S t_3} \mathrm{e}^{-\mathrm{i}H_S t}] + \mathrm{h.c.} \qquad (2.20)$$

which is equivalent to the expression given in ref 27, except that the rotating wave approximation was not employed here. Because of the interchange of the diabatic electronic states $|\psi_0\rangle$ and $|\psi_1\rangle$ along the torsional mode (cf. eq 2.3b), both components of the electric field, $\mathrm{e}^{+\mathrm{i}\omega_2 t}$ and $\mathrm{e}^{-\mathrm{i}\omega_2 t}$, need to be taken into account.

Adopting the system eigenstate representation and assuming Gaussian laser pulses as described in eq 2.11b, we can perform the time integrations in eqs 2.18 to 2.20 analytically. As is shown in Appendix B, one obtains for the doorway operators

$$D_e(\omega_1) = \sum_{a,b,d} |b\rangle\langle d| \sigma^{\mathrm{eq}}_{aa} \mu_{ba} \mu_{ad} \mathrm{e}^{-\alpha\tau_1^2[(\omega_1 - \omega_{ba})^2 + (\omega_1 - \omega_{da})^2]} \qquad (2.21)$$

$$D_g(\omega_1) = \frac{1}{2}\sum_{a,b,c} |c\rangle\langle a| \mu_{cb} \mu_{ba} \mathrm{e}^{-\alpha\tau_1^2[(\omega_1 - \omega_{ba})^2 + (\omega_1 - \omega_{bc})^2]} \times \{\sigma^{\mathrm{eq}}_{aa} + \sigma^{\mathrm{eq}}_{cc} + (\sigma^{\mathrm{eq}}_{aa} - \sigma^{\mathrm{eq}}_{cc}) \times \mathrm{erf}[\mathrm{i}\sqrt{\alpha/2}\tau_1(2\omega_1 - \omega_{ba} - \omega_{bc})]\} \qquad (2.22)$$

where $\sigma^{\mathrm{eq}}_{aa}$ is the equilibrium density matrix element pertaining to the ath eigenstate and $\mathrm{erf}(\mathrm{i}y)$ is the error function. The notation is chosen such that eigenstates $|a\rangle$ and $|c\rangle$ are associated with

the diabatic electronic ground state and $|b\rangle$ and $|d\rangle$ are associated with the first excited diabatic electronic state. The Gaussian functions contain the resonance conditions of the electronic transition, which depend on the laser frequencies and pulse durations. It is seen that short laser pulses cause transitions to many final states, thus leading to a spectrally broad signal. An analogous calculation yields for the window operator

$$W(\omega_2) = \sum_{c,b,d} |b\rangle\langle d| \mu_{bc}\,\mu_{cd} \{ \mathrm{e}^{-\alpha\tau_2^2[(\omega_2+\omega_{bc})^2+(\omega_2+\omega_{dc})^2]} - \mathrm{e}^{-\alpha\tau_2^2[(\omega_2-\omega_{bc})^2+(\omega_2-\omega_{dc})^2]} \} \quad (2.23)$$

which contains two resonance conditions because the rotating wave approximation was not employed. By neglecting the system−bath coupling during the field-free propagation and restricting ourselves for simplicity to the stimulated-emission contribution, the combination of eqs 2.17, 2.21, and 2.23 yields[34]

$$I(\omega_2, \Delta t) = 2\omega_2 \sum_{a,c} \sigma_{aa}^{\mathrm{eq}} \left| \sum_b \mu_{ab}\mu_{bc} \mathrm{e}^{-\alpha\tau_1^2(\omega_1-\omega_{ba})^2} \times \mathrm{e}^{-\mathrm{i}E_b\Delta t} \mathrm{e}^{-\alpha\tau_2^2(\omega_2-\omega_{bc})^2} \right|^2 \quad (2.24)$$

which reflects the three steps of a pump−probe experiment—preparation, propagation, and probing—in a particularly simple way.

In a similar way, the dispersed signal (eq 2.14) can be written in terms of the doorway−window formalism (eq 2.17). Here the window operator $W(\omega_2)$ is replaced by

$$W(\omega, \omega_2) = \frac{1}{2\pi} E^*_2(\omega) \int_{-\infty}^{\infty} \mathrm{d}t \int_0^{\infty} \mathrm{d}t_3\, E_2(t)\, \mathrm{e}^{\mathrm{i}(\omega t+\omega_2 t_3)} \times [\mathrm{e}^{\mathrm{i}H_S t} \mathrm{e}^{\mathrm{i}H_S t_3} \mu \mathrm{e}^{-\mathrm{i}H_S t_3} \mu \mathrm{e}^{-\mathrm{i}H_S t} - \mathrm{e}^{\mathrm{i}H_S t} \mu \mathrm{e}^{\mathrm{i}H_S t_3} \mu \mathrm{e}^{-\mathrm{i}H_S t_3} \mathrm{e}^{-\mathrm{i}H_S t}] + \mathrm{h.c.} \quad (2.25)$$

Adopting the system eigenstate representation and performing all time integrations, we obtain

$$W(\omega, \omega_2) = \frac{\mathrm{i}}{2\pi} \sum_{c,b,d} |b\rangle\langle d| \mu_{bc}\,\mu_{cd} \mathrm{e}^{-\alpha(t_2\Delta\omega)^2} \times \left\{ \mathrm{e}^{-\alpha\tau_2^2(\omega_{bd}-\Delta\omega)^2} \left(\frac{1}{\omega_2+\omega_{bc}+\mathrm{i}\epsilon} - \frac{1}{\omega_2-\omega_{dc}+\mathrm{i}\epsilon} \right) + \mathrm{e}^{-\alpha\tau_2^2(\omega_{bd}+\Delta\omega)^2} \left(\frac{1}{\omega_2-\omega_{bc}-\mathrm{i}\epsilon} - \frac{1}{\omega_2+\omega_{dc}-\mathrm{i}\epsilon} \right) \right\} \quad (2.26)$$

where $\Delta\omega = \omega_2 - \omega$ and ϵ is a positive infinitesimal number.

Equations 2.21 to 2.23 and 2.26 constitute our final expressions for the calculation of pump−probe spectra. It should be noted that operators D_g, D_e, and W need to be calculated only once and that both the Redfield propagation and the spectral calculation scale as N^2.

3. Numerical Results

3.1. Computational Details. In all calculations, we have assumed that the system density operator is initially given by

$$\sigma(0) = |\psi_0\rangle|\phi\rangle\langle\phi|\langle\psi_0| \quad (3.1)$$

where $|\phi\rangle$ denotes the vibrational ground state of the system Hamiltonian (eq 2.2). Furthermore, we have assumed zero temperature of the bath. Several test calculations for a temperature $T = 300$ K showed that the results change only in details but not qualitatively. The system Hamiltonian of the isomerizing molecule has been expanded in 2 diabatic states $|\psi_0\rangle$ and $|\psi_1\rangle$, 150 free-rotor states for the isomerization coordinate, and 24 harmonic oscillator states for the vibronic coordinate. The third diabatic state $|\psi_2\rangle$ needs to be considered only for the calculation of the window operator representing the excited-state absorption. To achieve numerical convergence for the propagation, it was sufficient to take into account the lowest $N = 110$ and 800 eigenstates for the single- and two-mode models, respectively. For the calculation of the window operators, more (i.e., 250 and 3400, respectively) eigenstates needed to be included to account for all resonant electronic transitions.

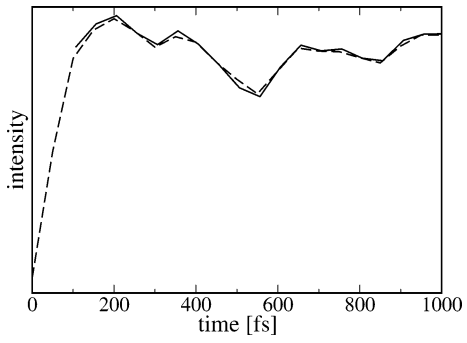

Figure 2. Comparison of the integral stimulated-emission signal at $\lambda_2 = 570$ nm as obtained by the doorway−window approximation (dashed line) and exact nonperturbative reference calculations (solid line). The latter results are shown only for times $\gtrsim$100 fs (i.e., when the pump and probe pulses are well separated in time).

To study the validity and accuracy of the doorway−window formulation, we have compared these results to exact nonperturbative simulations. As a representative example, Figure 2 shows the integral stimulated-emission signal at $\lambda_2 = 570$ nm obtained for the cis → trans photoisomerization of the single-mode model. The laser pulse durations were chosen as $\tau_1 = 35$ fs and $\tau_2 = 50$ fs, and the system−bath coupling $H_{\mathrm{SB}}^{\mathrm{T}}$ was considered. The perfect agreement of the two calculations suggest that the neglect of bath-induced dissipation during the pump and probe process is justified because the pulse durations are short on the time scale of the system−bath relaxation. The probe duration was increased up to 100 fs (data not shown), but no discrepancy between the signals was found. The computations of the data shown in Figure 2 took about 11 CPU days for the nonperturbative calculation and about 3 CPU seconds for the doorway−window calculation.

To be specific, throughout this paper the durations of the laser pulses will be chosen as $\tau_1 = 35$ fs and $\tau_2 = 20$ fs. Furthermore, we focus on the integral pump−probe signal (2.13). Although one usually finds that $I(\omega_2, \Delta t) \approx S(\omega = \omega_2, \Delta t)$, the two signals become different with increasing frequency difference $|\omega - \omega_2|$ because the dispersed spectrum is limited to the Fourier width of the probe pulse. To monitor the cooling process of hot photoproducts, which is reflected by the tails of the transient spectra, the integral pump−probe signal is therefore better suited.

3.2. Spectral Features of the Initial Coherent Photodynamics. As explained in the Introduction, transient transmission spectra typically reflect several spectral processes that often are hard to discriminate experimentally. In a theoretical description, however, this problem does not occur because the various spectral contributions are calculated separately. This is demonstrated in Figure 3, which displays all spectral contributions of the single-mode model with system−bath coupling $H_{\mathrm{SB}}^{\mathrm{T}}$

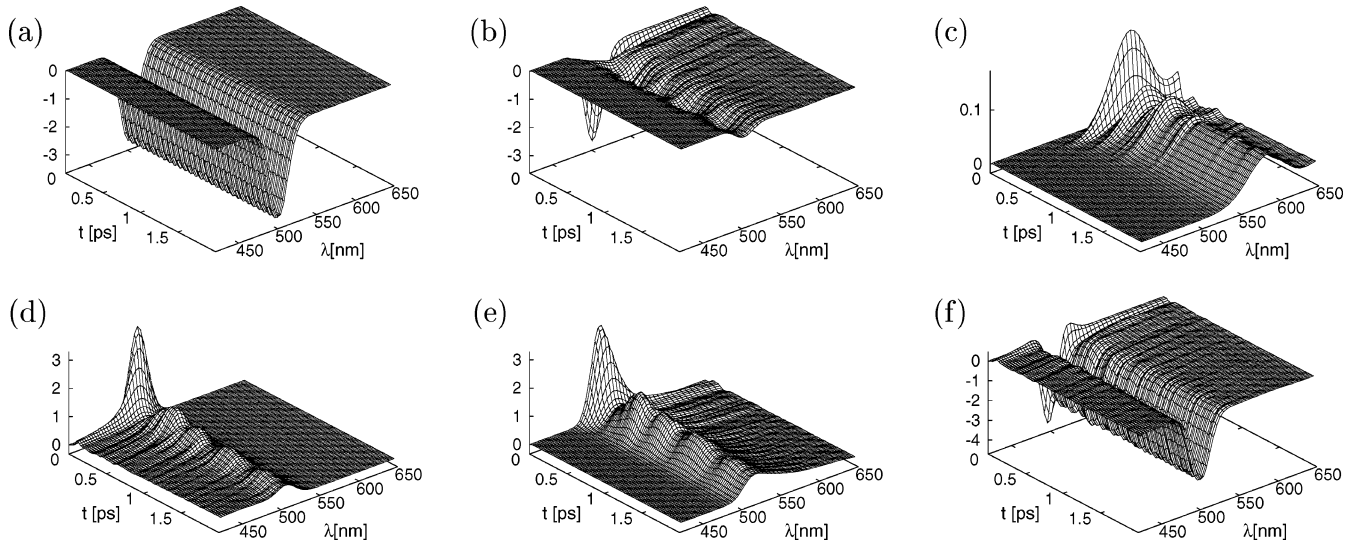

Figure 3. Contributions to the short-time transient absorption spectrum of the single-mode model. Shown are (a) the ground-state bleach, the stimulated emission and absorption arising from (b) the cis and (c) the trans configurations, the excited-state absorption obtained for (d) the standard model ($\tilde{V}_2 > 0$), and (e) an alternative model ($\tilde{V}_2 < 0$) as well as (f) the total transient absorption spectrum obtained as a sum of a−d. Note the different scales of the *z* axes, which account for the intensities of the various contributions.

shown for the first two picoseconds and wavelengths ranging from 420 to 650 nm.

The ground-state contribution to the signal is shown in Figure 3a. It reflects the bleach of the absorption band due to the reduced population in the ground state after excitation as well as stimulated Raman emission, which gives rise to a slightly coherent oscillation of the signal. Because the recovery of the ground state has hardly started within two picoseconds, the signal appears to be virtually stationary on this time scale.

Panels b and c show the stimulated emission ($S_1 \rightarrow S_0$) and absorption ($S_0 \rightarrow S_1$) occurring in the cis and the trans configurations, respectively. Following the excitation of the system by the pump pulse, the cis signal is dominated by stimulated emission that is centered at a wavelength of 500 nm. The cis signal also contains absorption in the red-shifted region ($\lambda > 550$ nm), reflecting the transient population of vibrationally excited states in the electronic ground state. In a time-resolved fluorescence experiment, the measured signal would solely consist of emission from the excited state. Such an experiment is therefore well suited to investigate the decay of the initially photoexcited chromophore. In the trans configuration, however, the excited electronic state is hardly populated because the excitation energy of the model is higher in the trans than in the cis configuration; see Figure 1. Therefore the trans signal contains only a hot absorption band whose maximum is red shifted to 570 nm. The absorption reaches far into the red ($\lambda >$ 650 nm), thus indicating highly excited vibrational states. Similar to the cis signal, the trans absorption shows oscillatory features reflecting the coherent wave packet motion of the system at early times.

Figure 3d shows the excited-state absorption of the model. Assuming for the higher-lying electronic state a vertical excitation energy of $E_2 = 4.91$ eV, we find that the absorption band is centered at 510 nm. Furthermore, we assume a torsional potential with $\tilde{V}_2 = 2.0$ eV, which causes the coordinate-dependent $S_1 - S_2$ energy gap to increase when the wave packet moves out of the Franck−Condon region; see Figure 1. As a consequence, the excited-state absorption signal in Figure 3d exhibits tails toward the blue spectral region. Because the structure of higher-lying electronic states is often known only poorly, it is interesting to investigate the sensitivity of the measured spectrum to the properties of this state. To this end, we consider an alternative model that gives the same absorption maximum for the $S_1 - S_2$ transition, but where $\tilde{V}_2 = -2.0$ eV. In this case, the $S_1 - S_2$ energy gap decreases when the wave packet leaves the Franck−Condon region. As a consequence, the excited-state absorption shown in Figure 3e exhibits tails toward the red. Apart from that, the excited-state absorption spectra obtained for the two quite different models are surprisingly similar.

Let us now consider the total transient absorption spectrum shown in Figure 3f, which typically is the only information accessible experimentally. We have assumed identical and constant dipole moments for all electronic transitions and for both configurations. Given as the sum of the signals in panels a−d, the total pump−probe spectrum during the first 2 ps is clearly dominated by the ground-state bleach at 500 nm. Only within the initial decay ($t \lesssim 200$ fs) are traces of the excited-state absorption and the stimulated emission readily observable.

A natural question that arises from the above discussion is to what extent the total transient absorption signal can be employed to extract information about the photoisomerization dynamics of the molecule. To answer that question, it is first helpful to introduce time-dependent observables that account for this process. A key quantity in the discussion of nonadiabatic cis−trans photoisomerization dynamics is the population probability[29]

$$P_k^{\text{trans}}(t) = \text{Tr}\{\sigma(t)\, P_{\text{trans}} |\psi_k^{\text{ad}}\rangle\langle\psi_k^{\text{ad}}|\} \qquad (3.2)$$

where

$$P_{\text{trans}} = \Theta(|\varphi| - \pi/2) \qquad -\pi/2 \le \varphi < 3\pi/2 \qquad (3.3)$$

denotes the projection operator onto the trans configuration and $|\psi_k^{\text{ad}}\rangle\langle\psi_k^{\text{ad}}|$ represents the projection operator onto the *k*th adiabatic state, which can be calculated from the diabatic states $|\psi_k\rangle$ through a unitary transformation.[14] Similarly, we may define the population probability $P_k^{\text{cis}}(t)$ via the operator $P_{\text{cis}} = 1 - P_{\text{trans}}$. Figure 4a shows the nonadiabatic cis−trans photoisomerization dynamics of the single-mode model as monitored by the observables $P_1^{\text{cis}}(t)$ and $P_0^{\text{trans}}(t)$. Clearly, the population probability $P_1^{\text{cis}}(t)$ reflects the decay of the initially prepared state, whereas $P_0^{\text{trans}}(t)$ monitors the build up of the photoprod-

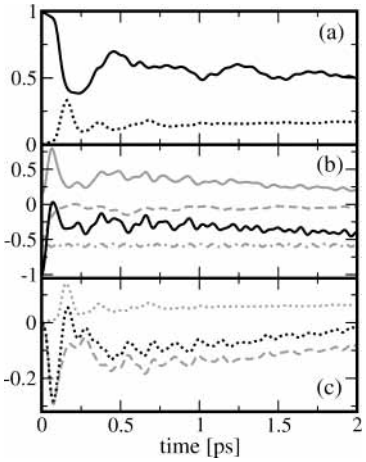

Figure 4. Nonadiabatic cis−trans photoisomerization dynamics of the single-mode model. (a) The population probability $P_1^{\mathrm{cis}}(t)$ (solid line) reflects the decay of the initially prepared state, whereas $P_0^{\mathrm{trans}}(t)$ (dotted line) monitors the build up of the photoproduct. The isomerization dynamics is reflected in the transient absorption of the system obtained at wavelengths of (b) 480 and (c) 570 nm. At 480 nm, the total spectrum (black solid line) is dominated by the excited-state absorption (grey solid line), and the ground-state bleach (grey dotted-dashed line) and the stimulated emission and absorption (grey dashed line) play a minor role. At 570 nm, the total spectrum (black dotted line) mainly reflects the stimulated emission and absorption of the cis configuration (grey dashed line), which cancels the trans absorption (grey dotted line).

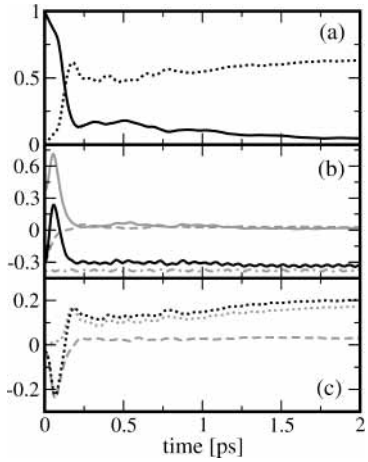

Figure 5. Same as in Figure 4, but for the two-mode model.

uct. The oscillatory structure of the observables results from quasiperiodic wave packet motion along the reaction potential curve.[35]

From the discussion above, it may be expected that the dynamics of the cis reactant is best monitored at a wavelength of 500 nm (corresponding to the cis $S_0 - S_1$ energy gap) and the dynamics of the trans product is best monitored at a wavelength of 570 nm (corresponding to the trans $S_0 - S_1$ energy gap). Whereas the latter is true, it proves advantageous to choose a wavelength of 480 nm to monitor the cis dynamics. As shown in Figure 4b, this is because at 480 nm the total signal is dominated by excited-state absorption whereas at 500 nm (data not shown) stimulated emission and excited-state absorption cancel each other almost completely. Although similar in its general features, the time evolution of the excited-state absorption directly reflects the delocalized motion of the wave packet around $\varphi = 0$ and therefore shows more oscillatory structure than $P_1^{\mathrm{cis}}(t)$.[35] At 570 nm, on the other hand, the total signal shown in Figure 4(c) is seen to be dominated by transient absorption in the cis configuration. Although the trans signal compares well with $P_0^{\mathrm{trans}}(t)$, the total signal at 570 nm hardly reflects the dynamics of the photoproduct as expected.

The above discussion appears to draw a somewhat pessimistic picture of the usefulness of transient pump−probe spectroscopy to interpret nonadiabatic cis−trans photoisomerization dynamics. However, it should be stressed that the example given above, on purpose, represents a worst-case scenario in several aspects for the following reasons. First, we have assumed a large spectral overlap of the various contributing spectroscopic processes. Although the energy gaps of the cis and trans configurations are indeed usually quite similar, the absorption region of higher-lying electronic states may be energetically well separated from the other absorption bands of the molecule. Moreover, because of the restriction of our model to one system mode, there is hardly a Stokes shift of the stimulated emission, which again would facilitate the interpretation. Second, we have assumed identical and constant dipole moments for all electronic transitions and for both configurations. Obviously, the interpretation becomes much easier if a single contribution dominates the spectrum. Whereas in a model calculation it is clearly an easy matter to choose parameters in such a way, it is important to note that there are also real systems that allow for a direct interpretation of the transient absorption signals. As an example, we mention the cis−trans photoisomerization of retinal in rhodopsin, which exhibits well-separated cis and trans spectral bands.[6]

Nevertheless, the data shown in Figure 4 suggest that even the single-contribution signals (e.g., the stimulated emission) only approximately match the corresponding population probability (e.g., $P_1^{\mathrm{cis}}(t)$). In particular, the spectral transients are additionally seen to contain oscillatory features. A closer analysis reveals that this finding is a consequence of long-lived excited-state coherences due to the 1D avoided crossing assumed in the model. The majority of real ultrafast photoisomerization reactions in polyatomic molecules, however, is assumed to occur through a multidimensional conical intersection.[3] Compared to avoided-crossing systems, conical intersection cause a significantly more efficient isomerization reaction and also suppress the coherent wave packet motion in the excited electronic state.[36] To demonstrate this effect, we have repeated the same analysis of the spectral lines at 480 and 570 nm for a two-mode model including a conical intersection. It should be emphasized that the energetics of the model is almost unchanged compared to that of the single-mode model (i.e., the spectral overlap of the various processes persists).

Figure 5 compares the population probabilities $P_1^{\mathrm{cis}}(t)$ and $P_0^{\mathrm{trans}}(t)$ and the various spectral signals at 480 and 570 nm as obtained for the two-mode model. The population probabilities shown in panel a directly reflect the much faster photoisomerization dynamics due to the conical intersection. The photoreaction is essentially finished within 200 fs. Interestingly, the total pump−probe signals at 480 and 570 nm are seen to follow the time evolution of the population probabilities quite nicely. The total signal at 480 nm is again dominated by the excited-state absorption, which for the two-mode model compares well with $P_1^{\mathrm{cis}}(t)$. From the initial decay of this signal, one may therefore directly draw conclusions on the reaction speed of the photoisomerization. Unlike the single-mode model, the total signal of the two-mode model at 570 nm is hardly affected by the stimulated emission from the cis configuration The total signal at 570 nm is therefore clearly dominated by the trans absorption signal, which reflects the build up of photoproduct.

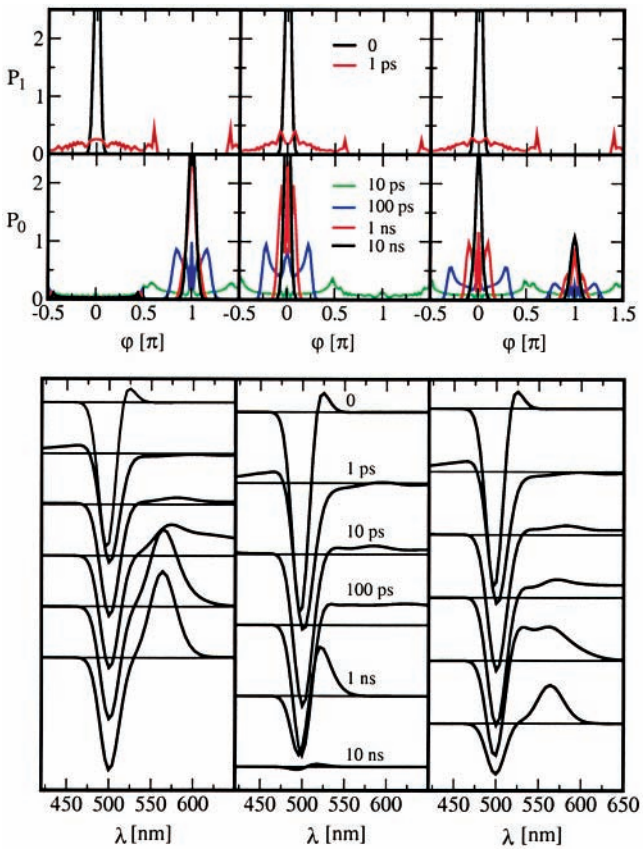

Figure 6. (Upper) Time-dependent probability density along the reaction coordinate in the excited (P_1) and ground (P_0) electronic states as obtained for the single-mode model. Three system−bath couplings are shown, which promote (left) the cis → trans reaction, (middle) the cis → cis back reaction, and (right) a mixture of the two reactions. (Lower) Corresponding transient absorption spectra.

3.3. Spectral Features of the Vibrational Cooling. During the first few picoseconds, the photoisomerization dynamics depends largely on the strong interactions contained in the system Hamiltonian but is little affected by the comparatively weak coupling to the bath. For example, we have seen a significant difference between the dynamics of the single-mode and two-mode models, but this dynamics change would be minor if a different system−bath coupling is assumed. (See below.) At longer times, the situation is reversed. The system is found in highly excited vibrational states of the adiabatic electronic ground state, and the main dynamical process that occurs is the vibrational cooling of the hot photoproducts due to the bath. In this case, the dynamics depends largely on the kind of the system−bath coupling that causes the cooling but is little affected by the details of the system. Therefore, in the following text, we again adopt the computationally less demanding single-mode model and study the long-time evolution of the system as a function of the system−bath coupling H_{SB}. As introduced in eq 2.5, we employ three types of coupling: H_{SB}^{T} promotes the cis → trans reaction, H_{SB}^{C} enforces the back reaction, and the symmetric coupling H_{SB}^{S} results in a mixture of cis and trans molecules and will be denoted as cis → cis/trans.

Before discussing the spectroscopic signals, it is instructive to investigate the vibrational relaxation dynamics obtained for the three bath types. This can be done by considering the time-dependent probability density along the reaction coordinate

$$P_k(\varphi, t) = \mathrm{Tr}\{\sigma(t)|\psi_k^{ad}\rangle|\varphi\rangle\langle\varphi|\langle\psi_k^{ad}|\} \qquad (3.4)$$

which is shown in the upper part of Figure 6. It should be noted that we plot only the density that has been excited by the pump pulse to the S_1 state because the density that remains in the electronic ground state is almost stationary and does not reflect the reaction dynamics.

After the excitation of the system by the pump pulse at time $t = 0$, the density is localized as a Gaussian wave packet around $\varphi = 0$ on the upper adiabatic state. After 1 ps, about half of the density is still in the S_1 state yet completely delocalized between $-0.7 \lesssim \varphi \lesssim 0.7\pi$. A comparison of the probability densities pertaining to the various system−bath couplings shows that in this initial phase the dynamics indeed is hardly influenced by the bath. At times $\gtrsim$10 ps, however, the system has almost completely decayed to the electronic ground state and starts to localize because of its interaction with the bath. As anticipated, the system−bath coupling H_{SB}^{T} affects the localization of the system in the trans configuration. The density is seen to move from the high-energy regions at the sides of the trans potential well (at $t = 10$ ps) to the middle of the well (at $t = 100$ ps) until the system is virtually in its vibrational ground state (at $t = 1000$ ps). Similarly, for the system−bath coupling H_{SB}^{C}, the system localizes in the cis configuration. Because the ground-state energy of the cis configuration is lower than the corresponding trans energy, the system is found to localize almost completely in the cis configuration for H_{SB}^{C} but only 80% in the trans configuration for H_{SB}^{T}. As may be expected, in the case of the system−bath symmetric coupling H_{SB}^{S}, the system localizes in both configurations, 60% in cis and 40% in trans.

The lower part of Figure 6 shows the transient absorption spectra as obtained for the three system−bath couplings. At time $t = 0$, the ground-state bleach and stimulated emission give rise to a prominent negative band centered at 500 nm. Furthermore, a small positive band at 520 nm is observed, which is due to excited-state absorption. At time $t = 1$ ps, the 500-nm band has become smaller because of the diminished stimulated emission (Figure 4). The red shift of the stimulated emission is indicated by a weak negative feature between 510 and 560 nm, which directly reflects the delocalization of the density on the excited electronic state. The excited-state absorption now shows up as a broad, blue-shifted band at $\lambda \lesssim 475$ nm. As expected, the transient absorption spectra obtained for the three system−bath couplings are quite similar up to this time.

At time $t = 10$ ps, the stimulated emission and the excited-state absorption have already decayed to zero, but the ground-state bleach is still virtually unaffected. Furthermore, a new absorption band emerges for $\lambda \gtrsim 520$ nm with a peak around 580 nm. This broad absorption band accounts for the vibrational cooling of the hot photoproduct. It is interesting that the overall appearance of the transient absorption spectra still does not reflect the configuration of the photoproduct, although at this time the system is already localized in the cis or trans configuration. The situation becomes clearer at time $t = 100$ ps, when a peak at 575 nm arises, reflecting the hot trans photoproduct in the case of the couplings H_{SB}^{T} and H_{SB}^{S}. In the case of cis localization due to H_{SB}^{C}, however, there is no maximum of the photoproduct absorption band because the ground-state bleach and the absorption of the hot cis molecules overlap to a large extent.

At even later times of the reaction, shown here for 1 and 10 ns, the cooling process affects a narrowing and a blue shift of the photoproduct absorption bands, which make the differences between the various system−bath couplings more pronounced. For the cis → trans reaction, for example, a blue shift from 580 nm at $t = 10$ ps to 570 nm at $t = 10$ ns is visible. Because the

quantum yield of the reaction is ~0.8, the remaining 20% cis population causes a remaining ground-state bleach at 500 nm. In the case of the cis → cis reaction, virtually all molecules react back to the cis configuration. The cooling process of the hot cis photoproduct is reflected in a decrease of the ground-state bleach on its red edge until it completely vanishes at $t =$ 10 ns. For the cis → cis−trans reaction, both effects are visible, the narrowing and blue-shifting absorption band of the trans product as well as the partial filling of the ground-state bleach due to the cis product.

4. Conclusions

We have outlined a theoretical formulation that allows us to calculate transient absorption spectra of photoreactive systems in the condensed phase. The formulation comprises a multidimensional model of nonadiabatic photoisomerization, a Redfield treatment of dissipation within the secular approximation, and a doorway−window formulation to calculate transient pump−probe spectra. Employing the eigenstate representation and assuming Gaussian laser pulses, explicit expressions for the doorway and window operators have been derived. The comparison to (numerically) exact nonperturbative reference calculations showed that the assumptions involved are well satisfied for the typical cases under consideration. As emphasized, the formalism scales with N^2 and therefore opens the way to treat multidimensional molecular models.

We have presented detailed computational studies of the dynamics and transient absorption of a number of cis−trans photoisomerization models. The simulations have shown that whereas the individual spectral contributions directly monitor the nonadiabatic photoisomerization process the interpretation of the total transient spectrum often will be complicated by overlapping spectral bands that effect a cancellation of the various spectral contributions. For the initial time evolution, it was found that only the two-mode model involving a conical intersection yields short-time spectral features as expected for a condensed-phase system. At later times, the dynamics is little affected by the details of the system but depends largely on the coupling of the chromophore to the environment. This interaction affects a vibrational cooling of the hot photoproducts that is typically reflected in broad absorption features that, however, only after a while reveal the nature of the photoproduct. In summary, the computational studies demonstrate the need for an appropriate theoretical modeling of femtosecond experiments in order to achieve a microscopic interpretation of transient absorption spectra of ultrafast photoreactions.

Appendix A. Discrimination of Spectral Contributions

In the nonperturbative calculation of the electronic polarization, special care has to be taken to separate the various spectral contributions occurring in the computed pump−probe signals. This is particularly true in the case of a nonadiabatically coupled system, where one needs to distinguish whether an electronic transition is caused by vibronic interactions or via the coupling to the radiation field. In ref 16, a symmetry property of the molecular system was invoked to perform this separation. In the general case, the following decomposition scheme may be employed.[37]

The principle is most easily explained in the wave function formalism. The basic idea is to decompose the total wave vector of the system into two terms:

$$|\Psi(t)\rangle = |\Psi_g(t)\rangle + |\Psi_e(t)\rangle \tag{A.1}$$

The partition is such that the wave vectors evolve from the interaction Hamiltonian $H_{\mathrm{int}}(t)$ according to

$$\mathrm{i}\frac{\partial}{\partial t}|\Psi_g(t)\rangle = H_{\mathrm{int}}(t)|\Psi_e(t)\rangle \tag{A.2a}$$

$$\mathrm{i}\frac{\partial}{\partial t}|\Psi_e(t)\rangle = H_{\mathrm{int}}(t)|\Psi_g(t)\rangle \tag{A.2b}$$

and from the system Hamiltonian H_{S} according to

$$\mathrm{i}\frac{\partial}{\partial t}|\Psi_k(t)\rangle = H_{\mathrm{S}}|\Psi_k(t)\rangle \tag{A.2c}$$

where $k = g, e$. That is, the external field causes transitions between $|\Psi_g(t)\rangle$ and $|\Psi_e(t)\rangle$, and the vibronic coupling causes transitions within $|\Psi_g(t)\rangle$ and $|\Psi_e(t)\rangle$, respectively. The decomposition of the wave function in eq A.1 thus allows us to discriminate between field-induced and vibronic-coupling-induced transitions.

Let us now assume that the system is initially in its vibronic ground state $|\Psi_0\rangle$ and that at this time only the $|\Psi_g\rangle$ state is prepared:

$$|\Psi(-\infty)\rangle = |\Psi_0\rangle = |\Psi_g(-\infty)\rangle \tag{A.3}$$

Following the preparation of the system by the pump laser into the state $|\Psi(t)\rangle$, the partition scheme (eq A.1) then allows us to separate spectral processes originating from the electronic ground state and the excited electronic state. The $|\Psi_e(t)\rangle$ component of $|\Psi(t)\rangle$ accounts for the fraction of molecules that have been prepared by the pump pulse in the excited electronic state. Upon the interaction with the probe pulse, this fraction will give rise to stimulated emission and excited-state absorption. Similarly, the $|\Psi_g(t)\rangle$ term accounts for the fraction of the molecules that are either left in the electronic ground state (yielding the bleach signal) or have been prepared by the pump pulse in the electronic ground state (yielding the stimulated Raman signal).

In the density-matrix formulation, the ideas outlined above lead to the ansatz

$$\sigma(t) = \sigma_g(t) + \sigma_e(t) + \sigma_{ge}(t) \tag{A.4}$$

where $\sigma_k = |\Psi_k\rangle\langle\Psi_k|$ $(k = g, e)$ and $\sigma_{ge} = |\Psi_g\rangle\langle\Psi_e| + |\Psi_e\rangle\langle\Psi_g|$. Assuming that initially $\sigma_g(-\infty) = \sigma^{\mathrm{eq}}$, the equations of motions read as

$$\frac{\partial}{\partial t}\sigma_k(t) = -\mathrm{i}[H_{\mathrm{int}}(t), \sigma_{ge}(t)] \qquad (k = g, e) \tag{A.5a}$$

$$\frac{\partial}{\partial t}\sigma_{ge}(t) = -\mathrm{i}[H_{\mathrm{int}}(t), \sigma_k(t)] \qquad (k = g, e) \tag{A.5b}$$

$$\frac{\partial}{\partial t}\sigma_i(t) = -\mathrm{i}[H_{\mathrm{M}}, \sigma_i(t)] \qquad (i = g, e, ge) \tag{A.5c}$$

which again facilitates the discrimination of field-induced and vibronic-coupling-induced transitions. By direct analogy to the wave function formulation explained above, after the pump pulse density operator $\sigma_g(t)$ accounts for the ground-state contributions, and density operator $\sigma_e(t)$ accounts for the excited-state contributions to the spectrum. Finally, it is interesting that in the limit of a weak laser field and negligible damping during the pulses the density matrices σ_g and σ_e are equivalent to the doorway operators $D_g(\omega_1)$ and $D_e(\omega_1)$.

Appendix B. Derivation of Equations 2.21−2.23

To derive the expression (eq 2.21) for the excited-state doorway operator $D_e(\omega_1)$, we insert system eigenstates in eq

2.18, yielding

$$D_e = \sum_{a,b,d} |b\rangle\langle d| \sigma_{aa}^{eq} \mu_{ba} \mu_{ad} \int_{-\infty}^{\infty} dt' \int_0^{\infty} dt_1 \, e^{i\omega_{bd}t'} \times [E^*_1(t') \, E_1(t-t_1) e^{-i\omega_{ba}t_1} + E_1(t') \, E^*_1(t'-t_1) e^{-i\omega_{da}t_1}] \quad \text{(B.1)}$$

By employing Gaussian laser fields (eq 2.11b) and performing the integration over t', we obtain

$$D_e = (8\pi\alpha\tau_1^2)^{-1/2} \sum_{a,b,d} |b\rangle\langle d| \sigma_{aa}^{eq} \mu_{ba} \mu_{ad} e^{-\alpha\tau_1^2\omega_{bd}^2/2} \times \int_0^{\infty} dt_1 \, e^{-t_1^2/(8\alpha\tau_1^2)} [e^{i(\omega_1 - \omega_{ba} + \omega_{bd}/2)t_1} + e^{i(\omega_1 - \omega_{da} - \omega_{bd}/2)t_1}] \quad \text{(B.2)}$$

By using the equality $\omega_1 - \omega_{ba} + \omega_{bd}/2 = \omega_1 - \omega_{da} - \omega_{bd}/2$, we can solve the integral over t_1, which gives

$$D_e = \sum_{a,b,d} |b\rangle\langle d| \sigma_{aa}^{eq} \mu_{ba} \mu_{ad} e^{-\alpha\tau_1^2\omega_{bd}^2/2} e^{-2\alpha\tau_1^2(\omega_1 - \omega_{ba} - \omega_{bd}/2)^2} \quad \text{(B.3)}$$

This expression is readily converted to the final result (eq 2.21) when the exponents are reorganized to give the resonance conditions $(\omega_1 - \omega_{ba})$ and $(\omega_1 - \omega_{da})$.

The window operator (eq 2.23) can be derived from eq 2.20 by complete analogy to the derivation above. The derivation of the ground-state doorway operator (eq 2.22), however, leads to a somewhat more complicated expression. Here, the expansion of eq 2.19 in the system eigenstate basis and integration over t' gives

$$D_g = (8\pi\alpha\tau_1^2)^{-1/2} \sum_{a,b,c} |c\rangle\langle a| \mu_{cb} \mu_{ba} e^{-\alpha\tau_1^2\omega_{ca}^2/2} \int_0^{\infty} dt_1 \, e^{-t_1^2/(8\alpha\tau_1^2)} \times [\sigma_{aa}^{eq} e^{i(\omega_1 - \omega_{ba} + \omega_{ca}/2)t_1} + \sigma_{aa}^{eq} e^{-i(\omega_1 - \omega_{bc} - \omega_{ca}/2)t_1}] \quad \text{(B.4)}$$

The analogy to eq B.2 is obvious, but the exponential terms in eq B.4 are weighted differently, which produces the following more elaborate expressions. Using the equality $\omega_1 - \omega_{ba} + \omega_{ca}/2 = \omega_1 - \omega_{bc} - \omega_{ca}/2$, integrating over t_1 with

$$\int_0^{\infty} dt_1 \, e^{-t_1^2/(8\alpha\tau_1^2) \pm i(\omega_1 - \omega_{ba} + \omega_{ca}/2)t_1} = \frac{1}{2}\sqrt{8\pi\alpha\tau_1^2} e^{-2\alpha\tau_1^2(\omega_1 - \omega_{ba} + \omega_{ca}/2)^2} \{1 - \mathrm{erf}[\mp i\sqrt{2\alpha}\tau_1(\omega_1 - \omega_{ba} + \omega_{ca}/2)]\} \quad \text{(B.5)}$$

and applying the symmetry relation $\mathrm{erf}(iy) = -\mathrm{erf}(-iy)$, we obtain

$$D_g = \frac{1}{2} \sum_{a,b,c} |c\rangle\langle a| \mu_{cb} \mu_{ba} e^{-\alpha\tau_1^2\omega_{ca}^2/2} \, e^{-2\alpha\tau_1^2(\omega_1 - \omega_{ba} + \omega_{ca}/2)^2} \times \{\sigma_{aa}^{eq} + \sigma_{cc}^{eq} + \mathrm{erf}[i\sqrt{2\alpha}\tau_1(\omega_1 - \omega_{ba} + \omega_{ca}/2)][\sigma_{aa}^{eq} - \sigma_{cc}^{eq}]\} \quad \text{(B.6)}$$

By reorganizing the exponents and using the equality

$$\omega_1 - \omega_{ba} + \frac{\omega_{ca}}{2} = \omega_1 - \frac{1}{2}(\omega_{ba} + \omega_{bc})$$

the final expression (eq 2.22) follows.

Acknowledgment. We thank Susanne Hahn, Michael Thoss, and Josef Wachtveitl for numerous inspiring and helpful discussions. This work has been supported by the Deutsche Forschungsgemeinschaft and the Fonds der Chemischen Industrie.

References and Notes

(1) Zewail, A. H. *J. Phys. Chem. A* **2000**, *104*, 5660.
(2) Michl, J.; Bonačić-Koutecký, V. *Electronic Aspects of Organic Photochemistry*; Wiley: New York, 1990.
(3) *Conical Intersections: Electronic Structure, Dynamics and Spectroscopy*; Domcke, W., Yarkony, D. R., Köppel, H., Eds.; World Scientific: Singapore, 2004.
(4) Radloff, W.; Stert, V.; Freudenberg, T.; Hertel, I. V.; Jouvet, C.; Dedonder-Lardeux, C.; Solgadi, D. *Chem. Phys. Lett.* **1997**, *281*, 20.
(5) Nägele, T.; Hoche, R.; Zinth, W.; Wachtveitl, J. *Chem. Phys. Lett.* **1997**, *272*, 489.
(6) Schoenlein, R. W.; Peteanu, L. A.; Wang, Q.; Mathies, R. A.; Shank, C. V. *Science* **1991**, *254*, 412.
(7) Du, M.; Fleming, G. R. *Biophys. Chem.* **1993**, *48*, 101.
(8) Kochendoerfer, G. G.; Mathies, R. A. *Isr. J. Chem.* **1995**, *35*, 211.
(9) Herbst, J.; Heyne, K.; Diller, R. *Science* **2002**, *297*, 822.
(10) Logunov, S. L.; Volkov, V. V.; Braun, M.; El-Sayed, M. A. *Proc. Natl. Acad. Sci. U.S.A.* **2001**, *98*, 8475.
(11) Kennis, J. T. M.; Larsen, D. S.; Ohta, K.; Facciotti, M. T.; Glaeser, R. M.; Fleming, G. R. *J. Phys. Chem. B* **2002**, *106*, 6067.
(12) Ye, T.; Friedman, N.; Gat, Y.; Atkinson, G. H.; Sheves, M.; Ottolenghi, M.; Ruhman, S. *J. Phys. Chem. B* **1999**, *103*, 5122.
(13) Bernardi, F.; Olivucci, M.; Robb, M. A. *Chem. Soc. Rev.* **1996**, *25*, 321.
(14) Domcke, W.; Stock, G. *Adv. Chem. Phys.* **1997**, *100*, 1.
(15) Mukamel, S. *Principles of Nonlinear Optical Spectroscopy*; University Press: Oxford, U.K., 1995.
(16) Seidner, L.; Stock, G.; Domcke, W. *J. Chem. Phys.* **1995**, *103*, 3998.
(17) Blum, K. *Density Matrix Theory and Applications*; Plenum: New York, 1981.
(18) May, V.; Kühn, O. *Charge and Energy Transfer Dynamics in Molecular Systems*; Wiley-VCH: Berlin, 2000.
(19) Fried, L. E.; Mukamel, S. *Adv. Chem. Phys.* **1993**, *84*, 435.
(20) Wolfseder, B.; Seidner, L.; Stock, G.; Domcke, W.; Seel, M.; Engleitner, S.; Zinth, W. *Chem. Phys.* **1998**, *233*, 323.
(21) Yang, M.; Ohta, K.; Fleming, G. R. *J. Chem. Phys.* **1999**, *110*, 10243.
(22) Ohta, K.; Yang, M.; Fleming, G. R. *J. Chem. Phys.* **2001**, *115*, 7609.
(23) Renger, T.; May, V.; Kühn, O. *Phys. Rep.* **2001**, *343*, 137.
(24) Pisliakov, A. V.; Gelin, M. F.; Domcke, W. *J. Phys. Chem. A* **2003**, *107*, 2657.
(25) In cases where the secular approximation breaks down, one may consider a computational scheme that accounts for the most important nonsecular terms (Balzer, B.; Stock, G. To be submitted for publication), thus retaining the N^2 behavior.
(26) Braun, M.; Meier, C.; Engel, V. *J. Chem. Phys.* **1995**, *103*, 7907.
(27) Yan, Y. J.; Mukamel, S. *Phys. Rev. A* **1990**, *41*, 6485.
(28) Hahn, S.; Stock, G. *J. Phys. Chem. B* **2000**, *104*, 1146.
(29) Seidner, L.; Domcke, W. *Chem. Phys.* **1994**, *186*, 27.
(30) Hahn, S.; Stock, G. *J. Chem. Phys.* **2002**, *116*, 1085.
(31) Note that the damping constants η_φ given in refs 30 and 36 by mistake are too large by a factor of 2.
(32) Walsh, A. M.; Coalson, R. D. *Chem. Phys. Lett.* **1992**, *198*, 293.
(33) Egorova, D.; Kühl, A.; Domcke, W. *Chem. Phys.* **2001**, *268*, 105.
(34) Stock, G.; Schneider, R.; Domcke, W. *J. Chem. Phys.* **1989**, *90*, 7184.
(35) Balzer, B.; Dilthey, S.; Hahn, S.; Thoss, M.; Stock, G. *J. Chem. Phys.* **2003**, *119*, 4204.
(36) Balzer, B.; Hahn, S.; Stock, G. *Chem. Phys. Lett.* **2003**, *379*, 351.
(37) Hahn, S. Ph.D. Thesis, Freiburg University, 2000.